# Opportunities and Challenges of Magnetic Seeded Filtration in Multidimensional Fractionation

**Frank Rhein*, Eric Schmid, Frederik Blase Esquivel, and Hermann Nirschl**

**DOI:** 10.1002/cite.201900104



Supporting Information available online

This study examines the general applicability of magnetic seeded filtration (MFS) for the fractionation of complex particulate systems by multiple particle features. Experimental studies on a laboratory scale showed that especially the electrostatic interactions govern the separation process. Furthermore, a clear size dependency could be shown, as the separation efficiency decreases with increasing size of target particles. Since MSF is both surface- and size-dependent, it is generally applicable in a multidimensional fractionation. Finally, the challenges to be overcome are addressed as well.

**Keywords:** Heteroagglomeration, Magnetic seeded filtration, Multidimensional fractionation, Solid-liquid separation

*Received:* July 22, 2019; *revised:* September 05, 2019; *accepted:* September 26, 2019

## 1 Introduction

Particle technology has made tremendous progress in recent years with more and more possible applications. Engineered nanoparticles (ENPs) are used in many industries ranging from the incorporation in tires to medicine [1, 2]. This naturally results in growing production figures which are unlikely to decline in the future [3]. Therefore, questions regarding the release and toxicity of such ENPs in the natural ecosystem arise and require addressing [4].

Particle separation technology has only been able to keep pace with this progress to a limited extent, although it is necessary both for the production and the recovery of such particles from the environment. As the demand for highly specific particle systems steadily grows, most separation techniques are optimized for a single particle feature. For example, filtration processes separate by size or classic magnetic separation apparatuses by susceptibility. In order to fractionate a particle mixture by multiple particle properties, traditionally a series connection of multiple separation steps is implemented, which increases costs and product loss. These drawbacks motivate the search for new techniques that are able to separate by multiple particle features simultaneously and, therefore, can be called multidimensional. This is a current field of research in separation technology [5], which is investigated by various groups, e.g. by density separation [6, 7].

This work focuses on multidimensional separation by magnetic seeded filtration (MSF). MSF is a less known two-step separation technology: In a first step, nonmagnetic (NM) target particles are agglomerated with magnetic seed particles. These heteroagglomerates can subsequently be separated due to their newly acquired magnetic properties. The multidimensionality lies in the first step, which is expected to be dependent both on surface properties and on the size of the target particles. Fig. 1 illustrates the general idea of magnetic seeded filtration in multidimensional separation: In the first step, only small NM1 particles agglomerate with the magnetic seed particles, while NM2 particles are excluded due to their incompatibility of surface properties and large NM1 particles due to their size. In the second step, the magnetic field is introduced resulting in the separation of the formed agglomerates.

As already mentioned, MSF is a lesser known technique, but has been implemented in some instances: It was used in the treatment of chemical mechanical polishing [8] as well as backside grinding [9] wastewaters and has achieved high

Frank Rhein, Eric Schmid, Frederik Blase Esquivel,
Prof. Dr.-Ing. Hermann Nirschl
frank.rhein@kit.edu
Karlsruhe Institute of Technology (KIT), Institute for Mechanical Process Engineering and Mechanics, Straße am Forum 8, 76131 Karlsruhe, Germany.

  

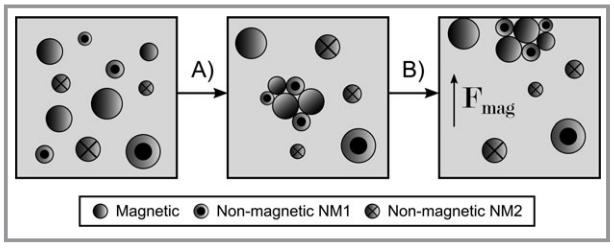


**Figure 1.** Process scheme of magnetic seeded filtration. A) (Selective) heteroagglomeration of magnetic and nonmagnetic particles. B) Magnetic separation of heteroagglomerates.

separation efficiencies for oppositely charged particle systems. Also, the implementation on larger scales was studied in the treatment of high turbid wastewater and showed promising results [10]. In a recently published article, MSF was used to separate microplastics from dilute suspensions [11]. However, all of these studies did not investigate the selectivity of the separation in a multicomponent suspension but intended the complete separation of nonmagnetic particles. Gray et al. [12] investigated the recovery of fine gold particles from mineral industry effluents by MSF and could demonstrate selectivity of the process. Furthermore, Förster et al. [13] found that nonmagnetic particles could be separated by heteroagglomeration with magnetic particles during the magnetic separation of oils and that there is a certain size dependency. However, the size dependency required for a possible multidimensional implementation has not yet been satisfactorily studied.

In the scope of this study, both the surface dependency as well as the size dependency of MSF are investigated. Initially, it is performed in the simplified case with a two-component suspension containing only one type of nonmagnetic and one magnetic particle system. Furthermore, the challenges of and prerequisites for a truly selective and multidimensional separation by MSF are critically discussed.

## 2 Material and Methods

### 2.1 Theory of Magnetic Seeded Filtration

As mentioned above MSF consists of two process steps: First, heteroagglomeration between magnetic and nonmagnetic particles is induced, which can be described by a reduced, simplified agglomeration kinetic according to Eq. (1).

$$\frac{\partial N_{i,j}}{\partial t} \propto N_i N_j \beta_{i,j} \alpha_{i,j} = N_i N_j k_{i,j} \tag{1}$$

$N_i$ and $N_j$ are the number concentrations of both agglomeration partners, $N_{i,j}$ is the number concentration of a resulting agglomerate, $\beta_{i,j}$ is the so-called collision frequency and $\alpha_{i,j}$ is the collision efficiency. The collision frequency vividly describes the probability that two particles collide and can either be flow- or diffusion-controlled. As a rough estimate, particle systems larger than 1 µm can be considered flow-controlled [14]; however, this is dependent on more parameters than just particles size. The collision efficiency vividly describes the probability that two particles agglomerate upon collision. Various models for calculating collision efficiencies exist [15, 16], which are not detailed in this work. However, the underlying main principle is the balancing of repulsive and attractive particle-particle interactions. Commonly, the so-called DLVO interactions, namely the electrostatic (repulsive) as well as van-der-Waals (attractive) potentials, are regarded. The product of $\beta_{i,j}$ and $\alpha_{i,j}$ can be combined to the agglomeration rate $k_{i,j}$.

Following agglomeration, the heteroagglomerates as well as magnetic primary particles are separated by magnetic separation. The driving mechanism of this subprocess is the magnetic force, which can be described according to Eq. (2) [17]

$$F_{mag} = \mu_0 V_P M \nabla H \tag{2}$$

where $\mu_0$ is the vacuum permeability, $V_P$ is the volume and $M$ the magnetization of the particles, while $\nabla H$ represents the magnetic field gradient. The magnetic force is proportional to the particle volume ($\sim r_P^3$) which limits the separation efficiency for small magnetic particles. This enables the MSF to perform a size-dependent classification, as increasingly large nonmagnetic particles will be harder to separate due to their increased drag. In order to still achieve any separation, high magnetic flux densities of $B = 0.2T - 0.5T$ are necessary [18] that can be produced by permanent magnets in order to reduce energy and cooling demands relative to electromagnets. As shown in Eq. (2), a large absolute field strength is not sufficient, as the field gradient is the decisive parameter. In high gradient magnetic separation (HGMS), the gradients are induced by a fine, ferromagnetic mesh that is introduced into the suspension during separation.

### 2.2 Experimental Studies

Generally, the experimental studies presented in this work are carried out in a two-component suspension in order to gain first insights into the general applicability of magnetic seeded filtration for a multidimensional separation approach. The relevant properties of the particle systems used are summarized in Tab. 1. Further details, including the preparation of the stock suspensions, are given in the Supporting Information (SI, Sect. S1).

Furthermore, the zeta potentials of the particle systems are crucial for the agglomeration process. They were measured in triplicate with the ZetaSizer Nano ZS (Malvern Instruments) at constant ionic strength and are shown in Fig. 2 (see SI for further details).

It should be emphasized in particular that the zeta potentials have different signs for low pH values, while both particle systems are strongly negatively charged for high pH values. This fact will be further discussed in a later section. The general experimental procedure is shown in Fig. 3.

  

**Table 1.** Properties of used particle systems

| | Magnetic (M) | Nonmagnetic (NM) |
|---|---|---|
| Material | $SiO_2$-MAG | $SiO_2$ |
| Manufacturer | microParticles GmbH, Berlin Germany | Quarzwerke GmbH, Frechen Germany |
| Median diameter $x_{50,3}$ [µm] | 0.56/0.96 | 2.49 |
| Dispersity | monodisperse (see SI Sect. S1) | polydisperse (see SI Sect. S1) |
| Particle shape | spherical (see Fig. 4a) | angular/irregular (see Fig. 4b) |
| Saturation magnetization $M_S$ [A m$^2$kg$^{-1}$] | 10 | 0.1 |

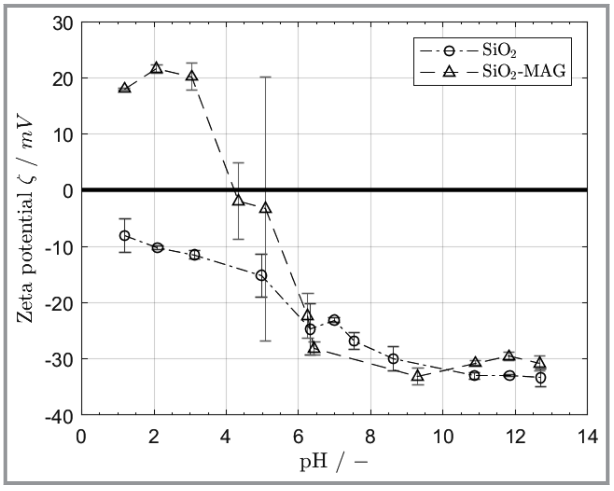


**Figure 2.** Zeta potential as function of pH for investigated particle systems.

First, the relevant volumes of magnetic and nonmagnetic stock suspension are added to a 25-mL snap-on lid vial. Then, 2 M analytic-grade sodium chloride (NaCl) solution was added to regulate the ionic strength. The pH value was adjusted by adding 0.5 M hydrochloric acid (HCl) or sodium hydroxide (NaOH). Finally, ultrapure water with a residual ionic strength of $10^{-6}$ M was added until the total volume of 25 mL was reached. The agglomeration step was carried out on the laboratory shaker IKA Vortex 3 at constant vibration intensity. This setup does not allow a clear quantification of the energy input into the system; however, the vibration intensity was neither varied nor its influence fundamentally studied during the experiments. In the given particle size range of < 10 µm, both flow-induced and diffusive collision are likely to be important. After 15 min of agglomeration time, the vial was placed on a permanent magnet and a ferromagnetic mesh was inserted. After the separation time of 2 min, the supernatant containing the not separated particles was collected and further analyzed. In order to quantify the concentration of nonmagnetic particles after the separation step, the samples were analyzed by photometric analysis at $\lambda$ = 600 nm. The validity of the Beer-Lambert law was ensured in previous studies so that the measured absorbance values can be transferred into concentration values through a calibration curve. Since the concentration before the agglomeration step is known, the overall separation efficiency can be calculated according to Eq. (3):

$$T_{NM} = \left(1 - \frac{c_{NM}(15\,\text{min})}{c_{NM}(0\,\text{min})}\right) \cdot 100\% \tag{3}$$

Furthermore, the supernatant was analyzed in the analytical disc centrifuge DC24000 (CPS Instruments Inc.) in order to gain information about the size dependency of the process. The size-dependent separation efficiency is given in Eq. (4) and is calculated for each particle size analogously to Eq. (3). Instead of concentration values, the relative weights yielded by the CPS measurements are used.

$$T_{NM}(x) = \left(1 - \frac{rW(x, 15\,\text{min})}{rW(x, 0\,\text{min})}\right) \cdot 100\% \tag{4}$$

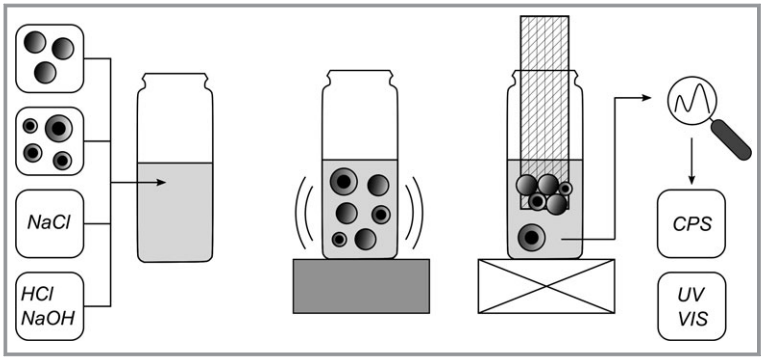


**Figure 3.** Experimental procedure consisting of four steps: sample preparation, agglomeration, separation, and analysis.

The general experimental parameters are summarized in Tab. 2. $x_{50,3,M}$ represents the median diameter of the used magnetic particle system, $c_{M,V}$ and $c_{NM,V}$ describe the volume concentrations of magnetic and nonmagnetic particles, respectively. $R_V$ and $R_N$ represent the resulting volume and number ratios (M/NM) and $t_{Agglo}$ the agglomeration time. As an agglomeration event can only occur upon collision and the absolute collision rate is dependent on particle number concentrations as shown in Eq. (1), it is

  

**Table 2.** General experimental parameters.

| Parameter | Setup 1 | Setup 2 |
|---|---|---|
| $x_{50,3,M}$ [µm] | 0.53 | 0.96 |
| $c_{M,V}$ [vol %] | $2.8 \cdot 10^{-3}$ | $1.39 \cdot 10^{-2}$ |
| $c_{NM,V}$ [vol %] | $3.8 \cdot 10^{-3}$ | $3.8 \cdot 10^{-3}$ |
| $R_V = V_M/V_{NM}$ [–] | 0.74 | 3.65 |
| $R_N = N_M/N_{NM}$ [–] | 14.77 | 14.77 |
| $t_{agglo}$ [min] | 15 | 15 |

evident that the number ratio $R_N$ between magnetic and nonmagnetic particles plays a crucial role. Therefore, when increasing the size of magnetic particles, this value and not the volume ratio is held constant. Note that perfect spheres and monodispersity are assumed for the calculation of $R_N$.

## 3 Results and Discussion

First, it had to be established that the separation is indeed based on a heteroagglomeration between the magnetic and nonmagnetic particles. In a first experiment, the supernatant was replaced by ultrapure water after the agglomeration step and all separated particles and agglomerates were redispersed. The redispersed sample was then examined using a scanning electron microscope (SEM). An example of such a recording is shown in Fig. 4a together with a SEM image of pure $SiO_2$ particles in Fig. 4b for reference. Due to the different particle shapes and sizes it becomes apparent that the separation of the angular and irregularly shaped $SiO_2$ particles can be retraced to the agglomeration with the spherical and monodisperse $SiO_2$-MAG particles. Furthermore, the small features on the surface of the $SiO_2$ particles, are likely smaller $SiO_2$ fragments that agglomerated due to the milling step in their production.

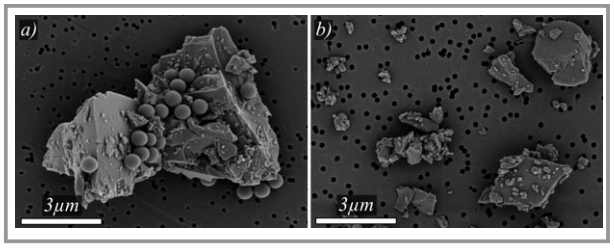


**Figure 4.** a) SEM image of a collected heteroagglomerate. Spherical particles: $SiO_2$-MAG; angular particles: $SiO_2$. Experimental setup 1 with $I$ = 1 M and pH = 11 (see Tab. 2). b) SEM image of pure $SiO_2$ particles as reference.

Furthermore, the entire experimental procedure was carried out without the addition of magnetic particles in a preliminary study. In this case, no separation of $SiO_2$ could be measured, which indicates that separation by sedimentation is negligible for the investigated system. After this proof of principle, the process-relevant properties and dependencies are investigated in the following sections.

### 3.1 Surface Dependency

The agglomeration of particles is known to be a surface-driven process. As mentioned above, the agglomeration rate $k_{i,j}$ mainly depends on the interplay of repulsive double layer and attractive van-der-Waals interactions. As such, the repulsive electrostatic interactions impede an agglomeration and should therefore be reduced. The surface potential as well as the ionic strength play a crucial role and are, thus, examined by the experimental studies. Fig. 5 shows the separation efficiency as a function of ionic strength and pH for experimental setup 1.

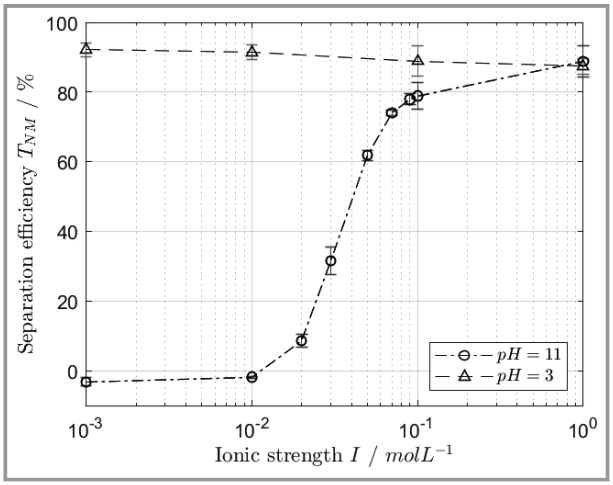


**Figure 5.** Separation efficiency as function of ionic strength and pH for experimental setup 1 (see Tab. 2).

It is evident that the separation for pH = 3 is almost independent of ionic strength and exhibits a constantly high efficiency of $T_{NM} \approx 90\,\%$. This phenomenon can be explained by the different signs of zeta potential, as shown in Fig. 2. At this pH, no repulsive interaction is present and the agglomeration between the particles is solely limited by collision.

In contrast, the separation at pH = 11 shows a strong dependency on the ionic strength: At low ion concentrations, no separation can be achieved. The marginally negative values can be explained by a small amount of magnetic particles that are not separated and increase the absorbance value. With increasing ionic strength, the separation efficiency also increases until $T_{NM} \approx 90\,\%$ for $I$ = 1 M is achieved again. This effect can be explained by the Debye length $\kappa^{-1}$ detailed in Eq. (5) [14]:

$$\kappa^{-1} = \sqrt{\frac{\varepsilon k_B \Theta}{2e^2 I N_a}} \tag{5}$$

The Debye length represents the distance to the surface, at which the surface potential is reduced in magnitude to

  

1/e times its value and can, therefore, be regarded as a measure for the range of the electrostatic interactions. For $I = 10^{-3}$ M, $\kappa^{-1}$ is approx. 10 nm, while for $I = 10^{-1}$ M, $\kappa^{-1}$ is already reduced to $\approx$ 1 nm. This reduction in range of the electrostatic repulsion results in an increased collision efficiency and overall separation efficiency at pH = 11.

### 3.2 Size Dependency

In order to achieve multidimensional separation, the heteroagglomeration further needs to be dependent on another particle property. This section covers the size dependency of the process. Therefore, the particle size distribution is measured before and after the experiment in the analytical disc centrifuge. In general, the separation efficiency is calculated as shown in Eq. (4). For further information on the CPS measurement and an exemplary evaluation please refer to SI Sect. S5. The first two curves are measured with experimental setup 1 for varying ionic strengths, while the third curve results from the experimental setup 2 with larger magnetic seed particles (see Tab. 2). The pH was held at 11 in all experiments. The chosen measurement range is $x_{\min}$ = 1 µm < $x$ < $x_{\max}$ = 10 µm, as the drop in separation efficiency is expected for large $SiO_2$ particles. Each of the three experiments presented in Fig. 6 was conducted three times. In addition, each sample was measured in triplicate and averaged by the built-in function of the CPS. The separation efficiencies for each experiment were averaged, however, the error bars representing the standard deviation are only displayed for every 200th data point, as there are many discrete $x$-values (> $10^3$). The scaling of the $x$-axis is determined by the above-mentioned measurement range of the CPS.

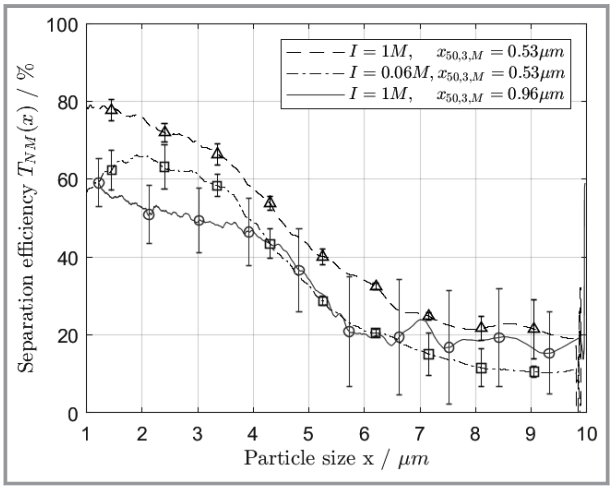


**Figure 6.** Separation efficiency as function of particle size for pH = 11. For clarity, the error bars are only shown for every 200th data point.

It is apparent that in all experiments the separation efficiency decreases significantly with increasing particle size of $SiO_2$. This effect might be due to two reasons: First, the magnetic force acting on the small magnetic particles is not sufficient to separate heteroagglomerates with large nonmagnetic particles. This implies that agglomeration is successful, but separation is not. Secondly, it is possible that no heteroagglomeration is taking place between small magnetic and large nonmagnetic particles. Such an effect could be explained by a decreasing collision frequency due to flow-controlled effects between these particles. Comparing both curves with experimental setup 1, the effect of ionic strength shown in Fig. 5 can be substantiated: An increase in ionic strength improves the overall separation efficiency without altering the general shape of the curves. As a logical consequence, the question arises whether it is possible to purposefully influence the size dependency. For this reason, the experiments were repeated with larger magnetic particles shown by the third curve in Fig. 6. Generally, the same trend of decreasing separation efficiency for larger nonmagnetic particles is observed, while the overall values are lower than for the corresponding experiment with smaller magnetic particles. This drop in separation efficiency may be retraced to the varying concentration ratios in the experiments. The assumption that the number ratio $R_N$ is the governing factor and that for constant $R_N$ the separation efficiencies will also be identical was shown to be inaccurate, although, the overall separation efficiencies are in a similar range. It can be challenging to discuss the effect on size dependency solely from Fig. 6. Therefore, the smoothed finite difference approximation for the derivative $\Delta T_{NM}(x)/\Delta x$ is given in Fig. 7.

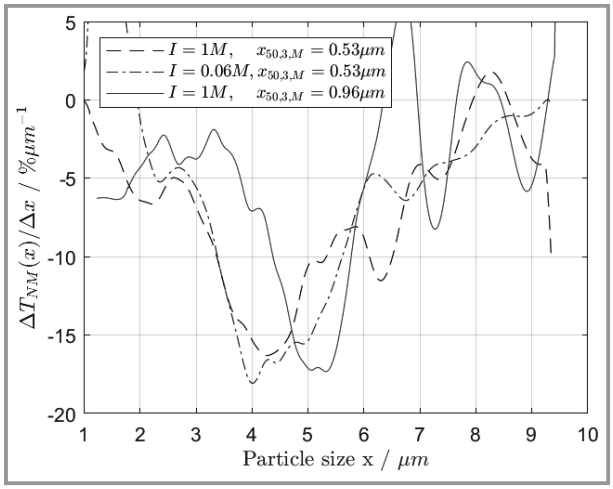


**Figure 7.** Numerical derivative of the separation efficiency as function of particle size.

Fig. 7 vividly describes the slopes and, thus, the general form of the curves in Fig. 6. First, it is evident that the variation of the ionic strength did not influence the size dependency, as both curves for small magnetic particles are nearly identical. However, it can be seen that for larger magnetic seed particles, the drop in separation efficiency occurs at larger particles ($x \approx$ 5 µm) than for smaller seed particles ($x \approx$ 4 µm). This can easily be harmonized with the explan-

  

ations given above: Both the absolute number of collisions (fixed $R_N$) and the collision efficiency (fixed $I$ and pH) were kept approximately constant, which should lead to a comparable occupation of the nonmagnetic particles with magnetic particles. However, larger magnetic particles correspond to an increased magnetic volume per nonmagnetic particle and, thus, to stronger magnetic forces in heteroagglomerates explaining the improved separation of larger nonmagnetic particles. In summary it could be shown that not only a clear size dependency exists in MSF, but also that this size dependency can be specifically controlled and regulated by careful selection of magnetic seed particles.

### 3.3 Thoughts on Selectivity

When transitioning to the three-component case shown in Fig. 1 by adding another nonmagnetic particle system, the selectivity of the process becomes the main parameter of interest. However, a selective separation based of surface charge is difficult, as an agglomeration process generally is not limited to one step. This is illustrated by the following example given in Fig. 8: Consider the nonmagnetic system 1 (NM1), which does not agglomerate with the magnetic system (M) due to similar surface charge and further, the nonmagnetic system 2 (NM2), which attaches to the magnetic particles due to opposing charge. In a second agglomeration step A2, the formation of three-component agglomerates is generally possible, since both nonmagnetic particles also tend to agglomerate with each other. The agglomeration rates $k_{i,j}$ shown in Fig. 8 are defined in Eq. (1) and indicate the probability of the respective agglomeration step.

NM1 will be separated through three-component agglomerates, resulting in a reduced selectivity towards NM2. In the following section, a rough calculation is performed under simplifying assumptions in order to gain first insights into the selectivity of the presented model case, which can be defined according to Eq. (6). Please note that the size dependency is not investigated in this model calculation.

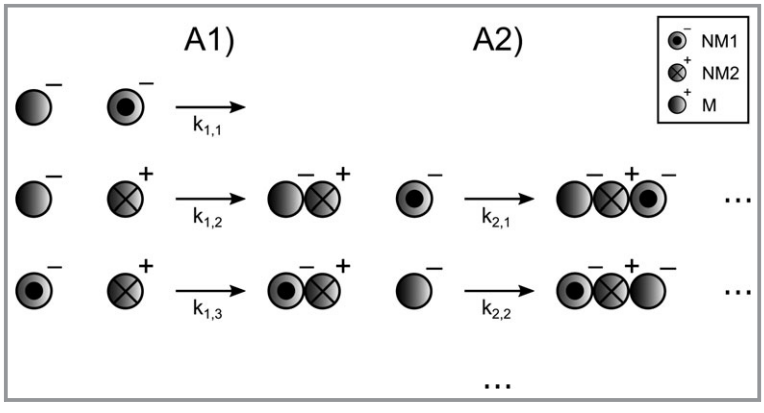


**Figure 8.** Illustration of selectivity issues in surface charge induced agglomeration. A1 refers to the initial agglomeration step of primary particles. A2 shows further agglomeration leading to three-component agglomerates.

$$S = 1 - \left(\frac{T_{NM1}}{T_{NM2}}\right) \tag{6}$$

Since NM2 is the target system in the presented case, selectivity reaches 1 when no NM1 is separated and 0 when NM1 and NM2 are separated equally. Furthermore, it is assumed that $T_{NM2} > T_{NM1} > 0$ resulting in $0 < S < 1$. A selective separation of NM2 can generally be accomplished if the agglomeration between NM1 and NM2 can be suppressed. Therefore, the ratio between both agglomeration rates $R_k = k_{1,3}/k_{1,2}$ is assumed to be of major importance. $R_k$ vividly describes the agglomeration tendency of NM2: $R_k > 1$ means that NM2 prefers to agglomerate with NM1, while $R_k < 1$ means that NM1 prefers to agglomerate with M. Furthermore, the kinetics of A2 are closely linked to the kinetics of A1 and especially limited in the beginning of an agglomeration process. Thus, the total agglomeration time could be another key factor for achieving selectivity.

Previous work [16] established the calculation on the basis of a validated discrete population balance equation. In this work, the model is extended to the 3D case, but also simplified, since the primary agglomeration efficiencies are predefined and held constant. In the following, the main assumptions necessary for understanding the results are outlined, but the used equations, indexing as well as model parameters are presented in detail in the SI, Sect. S6.

The numerical values of the primary collision efficiencies are $\alpha_{1,1} = 0$ (no agglomeration occurring) and $\alpha_{1,2} = 1$ (complete destabilization). The remaining primary collision efficiency is varied through $R_k$ according to $\alpha_{1,3} = R_k\alpha_{1,2}$. All collision efficiencies of higher order ($\alpha_{2,1}$,$\alpha_{2,2}$,…) can be estimated with the collision case model described in [16]. This model was previously validated and is only reliant on primary particle properties ($\alpha_{1,1}$,$\alpha_{1,2}$,$\alpha_{1,3}$) and agglomerate composition. The collision frequency depends on the mean shear rate in the system. Therefore, a scaling factor $\beta^*$ is introduced and varied on two levels $\beta_A^* = 10^3\,s^{-1}$ and $\beta_B^* = 10^4\,s^{-1}$. It is assumed that both nonmagnetic particle systems have the same size and all particle systems have the same initial volume concentration $c_V = 10^{-3}$ vol %. For simplification, all agglomerates containing at least one magnetic particle are assumed to be separated. This assumption seems to be in contrast to the results of Sect. 3.2, where it has been shown that a certain size-dependent minimum occupation of nonmagnetic with magnetic particles is necessary for separation. However, as these results aim to investigate the general selectivity, it appears to be more important that this assumption applies equally to all agglomerates rather than that the absolute value for this minimum occupation is correct. Furthermore, it is assumed that the dispersion step of the not separated suspension breaks up all nonmagnetic agglomerates after the process. The results of the calculations are shown in Figs. 9 and 10.

  

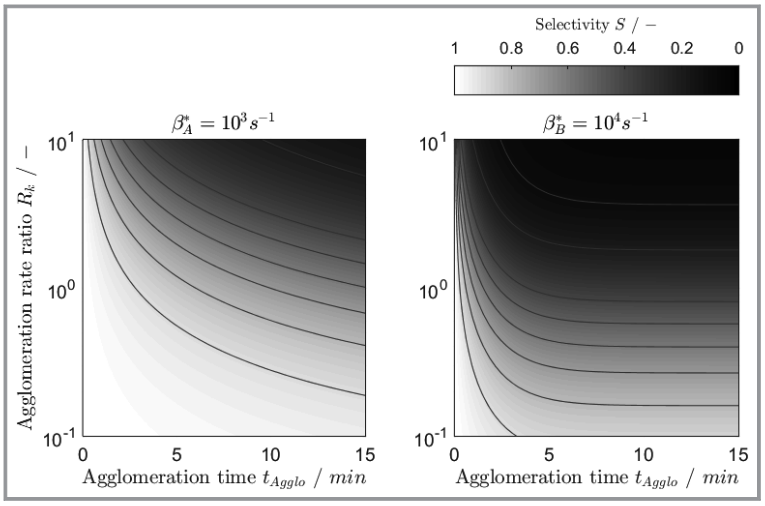


**Figure 9.** Selectivity $S$ as function of agglomeration time $t_{Agglo}$ and agglomeration rate ratio $R_k$. Results are shown for two levels of $\beta^*$. Left: $\beta_A^* = 10^3\ s^{-1}$, right: $\beta_A^* = 10^4\ s^{-1}$.

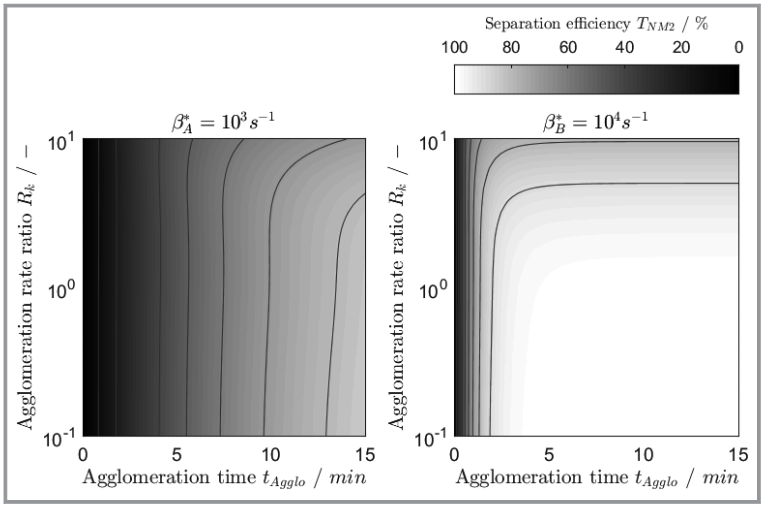


**Figure 10.** Separation efficiency of NM2 $T_{NM2}$ as function of agglomeration time $t_{Agglo}$ and agglomeration rate ratio $R_k$. Results are shown for two levels of $\beta^*$. Left: $\beta_A^* = 10^3\ s^{-1}$, right: $\beta_A^* = 10^4\ s^{-1}$.

First, it must be stated that no negative selectivity values are calculated, meaning that always more NM2 is separated than NM1 ($T_{NM2} > T_{NM1}$), which is to be expected as $k_{1,1} = 0$, while $k_{1,2} > 0$. Furthermore, Fig. 10 shows that the overall separation of NM2 is only influenced by the agglomeration time and the value of $\beta^*$, but not by $R_k$. Fig. 9 shows that high selectivity is achieved both for low values of $R_k$ as well as for short agglomeration times $t_{Agglo}$. This can readily be explained by the basic thoughts given above: Low $R_k$ means low agglomeration between both nonmagnetic particles, which is initially responsible for selectivity issues. However, $R_k$ is generally given by the surface properties of the nonmagnetic particle systems and is, therefore, not freely adjustable. Nevertheless, the calculations show that high selectivity independent of $R_k$ can be achieved when the agglomeration time is limited, since the formation of thee-component agglomerates can only occur after a sufficient amount of primary particle agglomeration. Increasing the value of $\beta^*$ and, thus, the agglomeration rates in general leads to higher overall separation efficiencies, but also to a reduction in selectivity at lower agglomeration times.

### 3.4 Outlook and Challenges

As shown above, magnetic seeded filtration exhibits both a clear surface as well as size dependency and is, thus, generally applicable to a multidimensional separation problem. A multicomponent system might be divided into classes of defined particle size as well as surface properties. However, the actual measurement of such multidimensional separation functions poses distinct challenges. By introducing a second nonmagnetic particle system, the suspension after the agglomeration step needs to be analyzed in such a way that size- and material-dependent concentration information can be accessed. Currently, this problem is addressed by transitioning from a single wavelength absorbance measurement to a UV-Vis spectral analysis, which should allow for material distinction given the materials exhibit different optical properties. However, as the optical properties are also known to be size-dependent, parallel size analysis will be crucial.

Model calculations indicate that selectivity can be achieved by adjusting the agglomeration time and/or the agglomeration rate between the two nonmagnetic systems. The latter may obviously be difficult to vary purposely as the nonmagnetic particles are predefined in real world problems. It may also be worth investigating other attractive interaction potentials that may be better suited for a selective agglomeration. In particular, hydrophobic interactions represent a promising path, since the agglomeration between both nonmagnetic particles and, therefore, also the problematic three-component agglomeration events might be inhibited entirely. However, it is difficult to find or modify suitable particle systems in order to investigate the problem profoundly.

Another focus of current research is the breakage of separated agglomerates, which is crucial for a recovery of magnetic particles as well as the separated nonmagnetic fraction. Nevertheless, it has been shown above that the agglomeration characteristics can be influenced drastically by simple adjustment of the suspension conditions (ionic strength, pH). Therefore, the process reversal and the breakage of agglomerates should also be possible if understood properly.

  

## 4 Conclusion

This study was concerned with the general applicability of magnetic seeded filtration as a multidimensional fractionation technique. On a laboratory scale, the crucial parameters for a surface-induced heteroagglomeration were clearly identified. In particular, the pH and ionic strength played a dominant role in the investigated particle systems. For oppositely charged particles, an almost complete separation of nonmagnetic particles could be achieved mainly independent of other parameters. However, the adjustment of the ionic strength also yielded high separation efficiencies for equally charged particles. As a second separation criterion, the particle size could be clearly identified as relevant. For magnetic seed particles of given size, the separation efficiency decreased for increasingly large nonmagnetic target particles. This was attributed either to a flow-induced reduction of collision frequency or to the fact that the magnetic force was insufficient to separate these large target particles. Furthermore, it was exemplarily shown that the size dependency can be specifically controlled and adjusted by the correct selection of magnetic seed particles. Due to the lack of analytical methods for a three-component system, model calculations were performed to provide insight into the selectivity of the process. It could be shown that especially the agglomeration time is a decisive factor for the selective separation in charge-controlled agglomerating systems.

The combination of both surface and size dependency should generally allow selective and multidimensional fractionation. However, this work also discussed general obstacles that have to be overcome. In particular, the selectivity of the surface charge-induced agglomeration requires further experimental investigations, as a compromise has to be made with the overall separation efficiency.

In conclusion, this work shows that magnetic seeded filtration is able to achieve high separation efficiencies in two-component suspensions and offers the prerequisites for an application in multidimensional fractionation.

The research project is funded by the DFG (German Research Foundation) in the priority program 2045 *Highly specific and multidimensional fractionation of fine particle systems with technical relevance*.

## Symbols used

| | | |
|---|---|---|
| $c_V$ | [vol %] | volume concentration |
| $e$ | [A s] | electron charge |
| $F$ | [N] | force |
| $H$ | [A m$^{-1}$] | magnetic field strength |
| $I$ | [mol m$^{-3}$] | ionic strength |
| $k$ | [–] | agglomeration rate |
| $k_B$ | [J K$^{-1}$] | Boltzmann constant |
| $M$ | [A m$^{-1}$] | magnetization |
| $N_a$ | [mol$^{-1}$] | Avogadro constant |
| $N_i$ | [m$^{-3}$] | number concentration |
| $R_k$ | [–] | agglomeration rate ratio $k_{1,3}/k_{1,2}$ |
| $R_N$ | [–] | number ratio magnetic/nonmagnetic |
| $R_V$ | [–] | volume ratio magnetic/nonmagnetic |
| $S$ | [–] | selectivity |
| $T$ | [%] | separation efficiency |
| $t_{Agglo}$ | [s] | agglomeration time |
| $V$ | [m$^3$] | volume |
| $x$ | [m] | particle diameter |
| $x_{50,3}$ | [m] | median diameter (weight) |

## Greek letters

| | | |
|---|---|---|
| $\alpha$ | [m$^{-3}$] | collision efficiency |
| $\beta$ | [m$^3$s$^{-1}$] | collision frequency |
| $\zeta$ | [V] | zeta potential |
| $\Theta$ | [K] | temperature |
| $\kappa^{-1}$ | [m] | Debye length |
| $\mu_0$ | [N A$^{-2}$] | vacuum permeability |

## References

[1] S. R. D'Mello, C. N. Cruz, M.-L. Chen, M. Kapoor, S. L. Lee, K. M. Tyner, *Nat. Nanotechnol.* **2017**, *12 (6)*, 523–529. DOI: https://doi.org/10.1038/nnano.2017.67

[2] R. Society, *Nanoscience and nanotechnologies: opportunities and uncertainties*, Latimer Trend Ltd, Plymouth **2004**.

[3] *Support for 3rd regulatory review on nanomaterials: Interim/Background Report*, Publications Office of the European Union, Luxembourg **2016**.

[4] B. Giese, F. Klaessig, B. Park, R. Kaegi, M. Steinfeldt, H. Wigger, A. von Gleich, F. Gottschalk, *Sci. Rep.* **2018**, *8 (1)*, 1–18. DOI: https://doi.org/10.1038/s41598-018-19275-4

[5] http://gepris.dfg.de/gepris/projekt/313858373?language=en (accessed on September 04, 2019)

[6] E. Schach, M. Buchmann, R. Tolosana-Delgado, T. Leißner, M. Kern, K. Gerald van den Boogaart, M. Rudolph, U. A. Peuker, *Miner. Eng.* **2019**, *137*, 78–86. DOI: https://doi.org/10.1016/j.mineng.2019.03.026

[7] S. E. Wawra, L. Pflug, T. Thajudeen, C. Kryschi, M. Stingl, W. Peukert, *Nat. Commun.* **2018**, *9 (1)*, 1–11. DOI: https://doi.org/10.1038/s41467-018-07366-9

[8] C.-J. M. Chin, P.-W. Chen, L.-J. Wang, *Chemosphere* **2006**, *63 (10)*, 1809–1813. DOI: https://doi.org/10.1016/j.chemosphere.2005.09.035

[9] T.-J. Wan, S.-M. Shen, S.-H. Siao, C.-F. Huang, C.-Y. Cheng, *Water Res.* **2011**, *45 (19)*, 6301–6307. DOI: https://doi.org/10.1016/j.watres.2011.08.067

[10] C.-J. M. Chin, Z.-G. Fan, *J. Environ. Eng. Manage.* **2010**, *20 (3)*, 145–150.

[11] F. Rhein, F. Scholl, H. Nirschl, *Chem. Eng. Sci.* **2019**, *207*, 1278–1287. DOI: https://doi.org/10.1016/j.ces.2019.07.052

[12] S. R. Gray, D. E. Langberg, N. B. Gray, *Int. J. Miner. Process.* **1994**, *41 (3)*, 183–200. DOI: https://doi.org/10.1016/0301-7516(94)90027-2

  

[13] E. Förster, A. Schmidt, F. Rhein, H. Anlauf, H. Nirschl, *Chem. Eng. Technol.* **2016**, *39 (3)*, 477–483. DOI: https://doi.org/10.1002/ceat.201500343
[14] M. Elimelech, *Particle deposition and aggregation : measurement, modelling and simulation*, Colloid and surface engineering series, Butterworth-Heinemann, Woburn, MA **1998**.
[15] N. Fuchs, *Z. Phys.* **1934**, *89 (11)*, 736–743. DOI: https://doi.org/10.1007/BF01341386
[16] F. Rhein, F. Ruß, H. Nirschl, *Colloids Surf., A* **2019**, *572*, 67–78. DOI: https://doi.org/10.1016/j.colsurfa.2019.03.089
[17] J. Svoboda, *Magnetic Techniques for the Treatment of Materials*, Springer Netherlands, Dordrecht **2004**.
[18] K. Menzel, C. W. Windt, J. A. Lindner, A. Michel, H. Nirschl, *Sep. Purif. Technol.* **2013**, *105 (Supplement C)*, 114–120. DOI: https://doi.org/10.1016/j.seppur.2012.12.019

  